Spectrum Adjustment Results for Three Environments in the ACRR Central Cavity Using a Genetic Algorithm

Richard M. Vega[1] and Edward J. Parma[2]

Abstract

Presented in this report is the description of a new method for neutron energy spectrum adjustment which uses a genetic algorithm to minimize the difference between calculated and measured reaction probabilities. The measured reaction probabilities are found using neutron activation analysis. The method adjusts a trial spectrum provided by the user which is typically calculated using a neutron transport code such as MCNP [1]. Observed benefits of this method over currently existing methods include the reduction in unrealistic artefacts in the spectral shape as well as a reduced sensitivity to increases in the energy resolution of the derived spectrum. This report presents the adjustment results for various spectrum altering bucket environments in the central cavity of the Annular Core Research Reactor. In each case, the results are compared to those generated using LSL-M2, which is a code commonly used for the purpose of spectrum adjustment [2]. The genetic algorithm produces spectrum-averaged reaction probabilities comparable to those resulting from LSL-M2. The true benefit to this method, the reduction of shape artefacts in the spectrum, is difficult to quantify but can be clearly seen in the comparison of the final adjustments.

Keywords

Annular Core Research Reactor, neutron spectrum adjustment, genetic algorithm

[1] R&D Graduate Year Round Intern, Applied Nuclear Technologies, Sandia National Laboratories[3], P.O. Box 5800, MS 1146, Albuquerque, New Mexico 87185, USA
[2] Principal R&D Scientist and Engineer, Applied Nuclear Technologies, Sandia National Laboratories[3], P.O. Box 5800, MS 1146, Albuquerque, New Mexico 87185, USA
[3] This work was performed for the U. S. Department of Energy at Sandia National Laboratories. Sandia National Laboratories is a multi-mission laboratory managed and operated by Sandia Corporation, a wholly owned subsidiary of Lockheed Martin Corporation, for the U.S. Department of Energy's National Nuclear Security Administration under contract DE-AC04-94AL85000.

Introduction

Spectrum adjustment is the process of taking a computed neutron energy spectrum, and adjusting it so that it is more consistent with experimental results. The computed spectrum, also called the trial spectrum, is typically calculated using computational neutron transport methods, and hence is prone to model errors, numerical errors, and data uncertainties. Still, the computed spectrum is often the best guess at the true spectrum, as it is typically impossible to measure the neutron energy spectrum in a reactor with high resolution. The experimental data used in spectrum adjustment consists of detector responses or neutron activation analysis (NAA). These experimental measurements are integral quantities of the product of the neutron energy spectrum and an energy dependent response function. In the case of NAA, the energy dependent response function is the reaction cross section unique to the activation foil being used.

Spectrum adjustment is inherently an under-determined problem if a high resolution spectrum is desired as the final product. Treating the flux in each energy group as a variable, the integral quantities that result from detector readings or dosimetry foils each correspond to a single equation. Typically, the number of energy groups desired is in the hundreds, while the number of practical detectors or dosimetry foils is less than 50. The desire to know the spectrum as accurately as possible stems from the desire to know other integral quantities (such as DPA and flux above or below a certain threshold energy) as accurately as possible. While modern Monte Carlo neutron transport codes can take advantage of parallel architectures to calculate neutron energy spectra with extremely high resolution and very little statistical variance in the flux values, model errors such as material temperature and composition uncertainties are unavoidable, as are the uncertainties associated with the transport and dosimetry cross sections used to compute the trial spectrum and reaction rates respectively.

Theory

Genetic algorithms have been used in recent decades to solve logistics problems such as the traveling salesman, word matching, and number partitioning problems. This abstract stochastic method has been gaining popularity steadily in the past decade and has made its way into the world of engineering as evidenced by NASA's use of a genetic algorithm for antenna design [3]. If a problem can be abstracted to a set of genes with a clear fitness function, a genetic algorithm will likely be applicable.

The genetic algorithm is essentially a simulation designed to mimic natural selection. The simulation starts with a population of possible solutions, or specimens, and each specimen is assigned a fitness value based on what makes any single specimen favorable over any other. The specimens are then chosen for mating in such a way that higher fitness specimens are selected for mating more frequently. The mating of these specimens produces children specimens which carry onto the next generations and hopefully carry the favorable characteristics of their parents with them. The process is then repeated for a prescribed number of generations.

If a genetic algorithm is successful, the fitness of the population as a function of generations will increase in its minimum, maximum, and average. At a certain point, convergence will be achieved, and the fitness levels of the population will cease to rise any further. If a genetic algorithm is to show these symptoms of success, the individual processes required to initiate and

propagate the specimens through the generations must be chosen wisely. These processes include representing the solution as a set of genes, setting the initial population, designing the fitness function, selecting the parents, mating the parents, and mutating the children. For details on the particular implementation of these processes in the genetic algorithm used here, the reader is referred to SAND2015-11036 [4].

Results

The Annular Core Research Reactor (ACRR) is the successor of the Annular Core Pulse Reactor (ACPR) which used standard TRIGA fuel in a hexagonal lattice surrounding a large dry cavity at the center of the reactor. The only difference between the two reactors is the fuel material. The ACRR uses UO_2BeO fuel which allows for a larger heat capacity so that it can sustain larger pulses. Figure 1 shows the ACRR lattice as modelled in MCNP. It can operate at steady state with power levels up to 4 MW, and can achieve a maximum pulse of 300 MJ with a full-width half-maximum of 6 ms. The ACRR was designed to have an epithermal spectrum which is a compromise between the thermal spectra of a light water TRIGA reactor, and the fast spectrum of a gas cooled reactor. It was designed this way so that different buckets could be placed in the central cavity to reproduce thermal or fast spectra depending upon the bucket materials.

The first set of results presents the adjustment of the free field spectrum; the spectrum in the central cavity with no bucket used to alter the spectrum. Further details on the ACRR can be found in SAND2006-3067 [5]. All LSL-M2 adjustment results used here for comparison to GenSpec were recently obtained as part of the free field characterization in SAND-2015-6483 [6]. The adjustments resulting from using the same trial spectrum and experimental measurements in LSL-M2 and GenSpec with an 89 group energy grid are shown in Figure 2. The adjustments performed using GenSpec for the 89 and 640 group energy grids are shown in Figure 3. Table 1 shows the measured and calculated reaction probabilities for both GenSpec and LSL-M2.

The second set of results presents the adjustment of the LB44 spectrum. The purpose of the LB44 bucket is to filter out low-energy neutrons via absorption in boron. Because of this absorption, the bucket has a reactivity worth of -$6.07 compared to the free field environment. In addition to filtering out low-energy neutrons from the spectrum, the lead layer is able to attenuate the gamma-ray fluence. Figure 4 shows the details of the LB44 bucket. Further details on the LB44 bucket can be found in SAND2013-3406 [7]. All LSL-M2 adjustment results used for comparison to GenSpec were obtained as part of the LB44 bucket characterization in SAND-2013-3406 as well. The adjustments resulting from using the same trial spectrum and experimental measurements in LSL-M2 and GenSpec with an 89 group energy grid are shown in Figure 5. The adjustments performed using GenSpec for the 89 and 640 group energy grids are shown in Figure.6. Table 2 shows the measured and calculated reaction probabilities for both GenSpec and LSL-M2.

The final set of results presents the adjustment of the PLG spectrum. The purpose of the PLG bucket is to produce more low-energy neutrons via scattering with hydrogen in the high-density polyethylene (HDPE) layer. In addition to increasing this low-energy component, the lead layer is able to attenuate the gamma-ray fluence. Figure 7 shows the details of the PLG bucket. Further details on the PLG bucket can be found in SAND2015-4844 [8]. All LSL-M2 adjustment results

used for comparison to GenSpec were obtained as part of the PLG bucket characterization in SAND-2015-4844 as well. The adjustments resulting from using the same trial spectrum and experimental measurements in LSL-M2 and GenSpec with an 89 group energy grid are shown in Figure 8. The adjustments performed using GenSpec for the 89 and 640 group energy grids are shown in Figure 9. Table.3 shows the measured and calculated reaction probabilities for both GenSpec and LSL-M2.

Tables 1 through 3 indicate that similar agreement with experimentally obtained results are obtained from both the genetic algorithm and LSL-M2, which uses a logarithmic least squares method. Figures 2, 5, and 8 indicate that the adjustments from both methods result in similar spectra, with the exception that the genetic algorithm produces a smooth adjustment devoid of artificial peaks and valleys that can only be artefacts of the adjustment process. Future work will include a stochastic method to provide uncertainties in the adjusted spectrum from the genetic algorithm.

References

1. MCNP-A General Monte Carlo N-Particle Transport Code, Version 5, Technical Report LA-UR-03-1987 (2003)

2. F. W. Stallmann, "LSL-M2: A Computer Program for Least-Squares Logarithmic Adjustment of Neutron Spectra," Technical Report NUREG/CR-4349, ORNL/TM-9933 (1985)

3. G. S. Hornby, J. D. Lohn, and D. S. Linden, "Computer-Automated Evolution of an X-Band Antenna for NASA's Space Technology 5 Mission," MIT Press, 19, pp. 1–23 (2011)

4. R. M. Vega and E. J. Parma, "GenSpec: A Genetic Algorithm for Neutron Energy Spectrum Adjustment," Technical Report SAND2015-11036 (2015)

5. K. R. DePriest, P. J. Cooper, E. J. Parma, "MCNP/MCNPX Model of the Annular Core Research Reactor," Technical Report SAND2006-3067 (2006)

6. E. J. Parma, G. E. Naranjo, R. M. Vega, L. L. Lippert, D. W. Vehar, P. J. Griffin, "Radiation Characterization Summary: ACRR Central Cavity Free-Field Environment with the 32-Inch Pedestal at the Core Centerline (ACRR-FF-CC-32-cl)," Technical Report SAND2015-6483 (2015)

7. E. J. Parma, T. J. Quirk, L. L. Lippert, P. J. Griffin, G. E. Naranjo, S. M. Luker, "Radiation Characterization Summary: ACRR 44-Inch Lead-Boron Bucket Located in the Central Cavity on the 32-Inch Pedestal at the Core Centerline (ACRR-LB44-CC-32-cl)," Technical Report SAND2013-3406 (2013)

8. E. J. Parma, D. W. Vehar, L. L. Lippert, P. J. Griffin, G. E. Naranjo, S. M. Luker, "Radiation Characterization Summary: ACRR Polyethylene-Lead-Graphite (PLG) Bucket Located in the Central Cavity on the 32-Inch Pedestal at the Core Centerline (ACRR-PLG-CC-32-cl)," Technical Report SAND2015-4844 (2015)

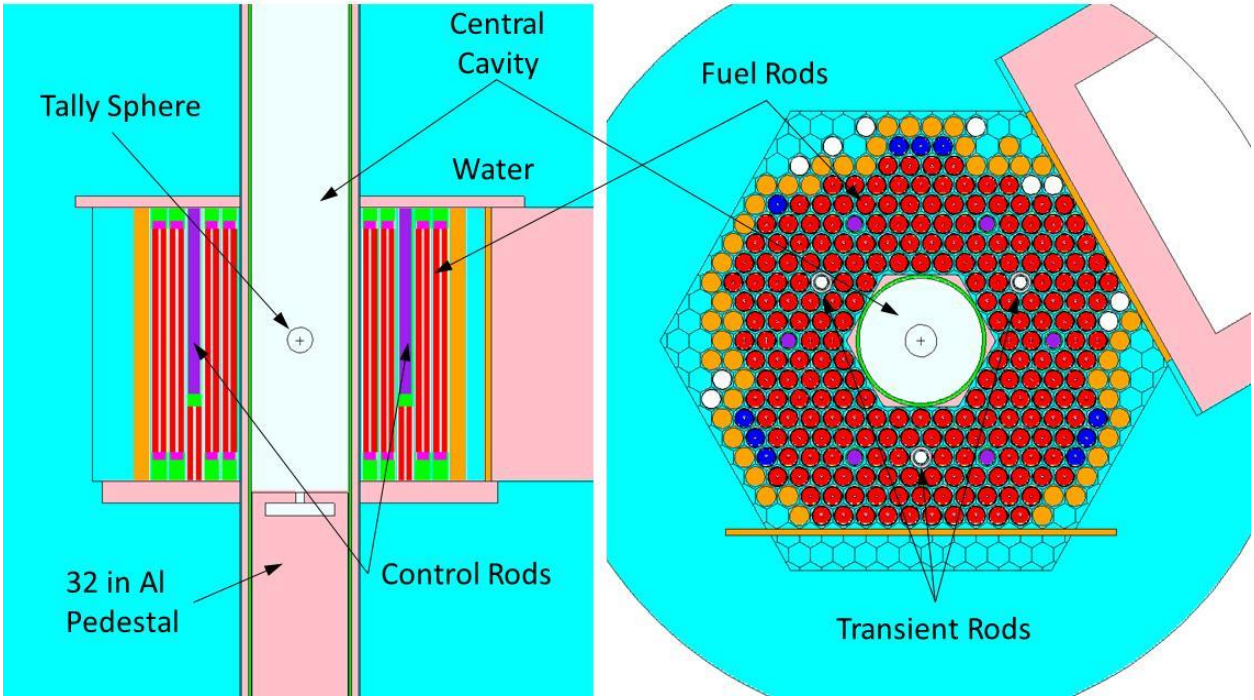

Fig. 1. MCNP Model of the ACRR and the Central.

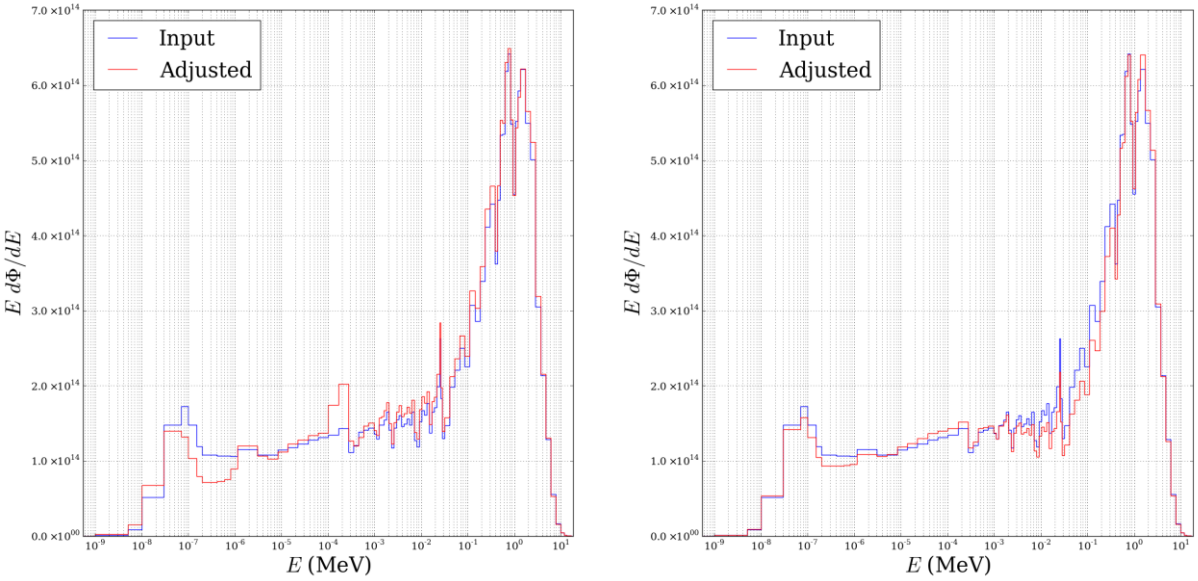

Fig. 2. Comparison of the adjustments performed using the 89 energy group structure for LSL-M2 (left) and GenSpec (right) for the free field environment in the central cavity of the ACRR.

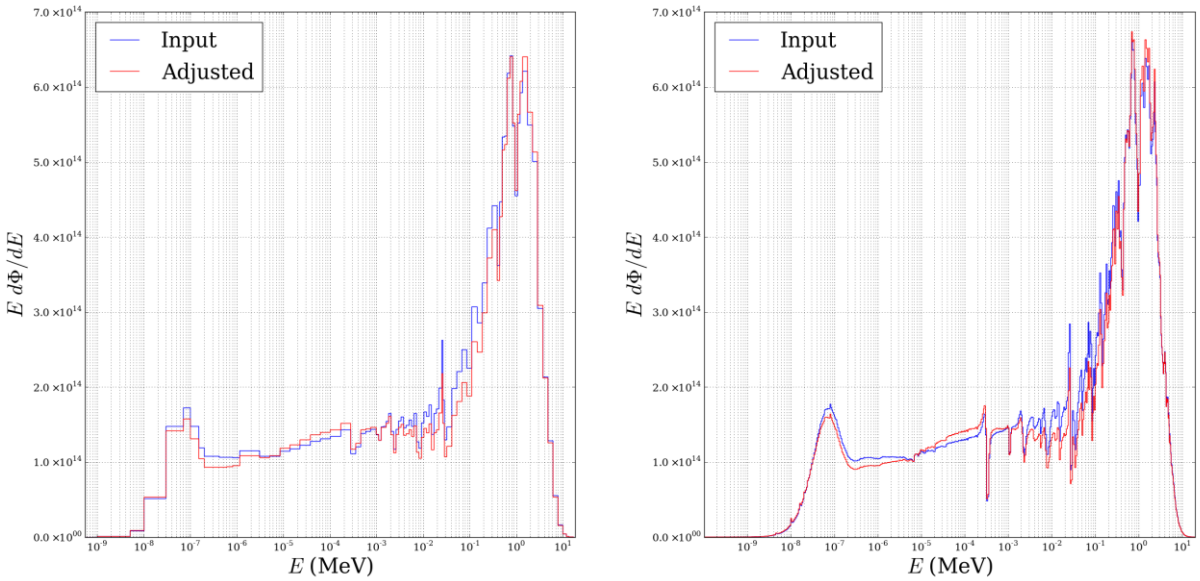

Fig. 3. Comparison of the adjustments performed using GenSpec for the 89 group (left) and 640 group (right) structures for the free field environment in the central cavity of the ACRR.

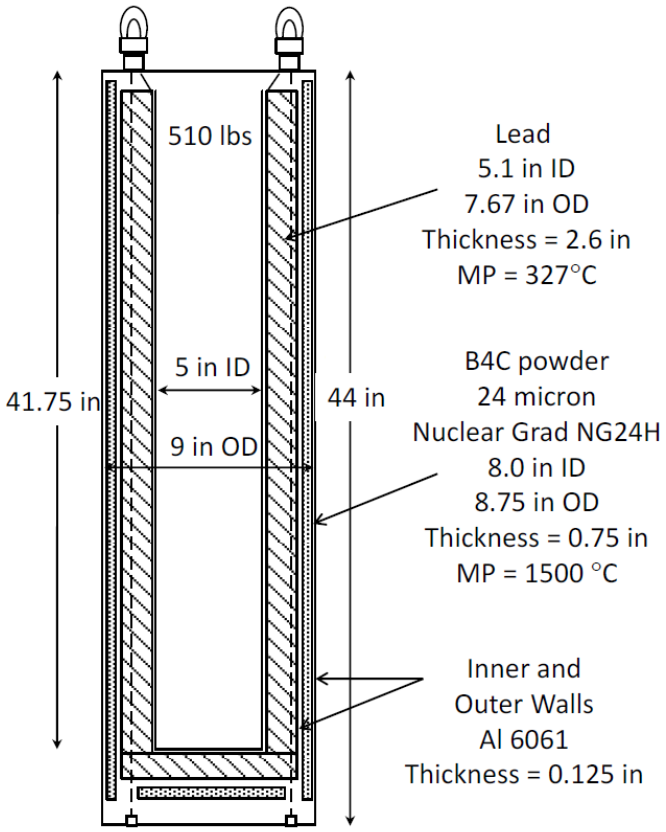

Fig. 4. Details of the LB44 bucket.

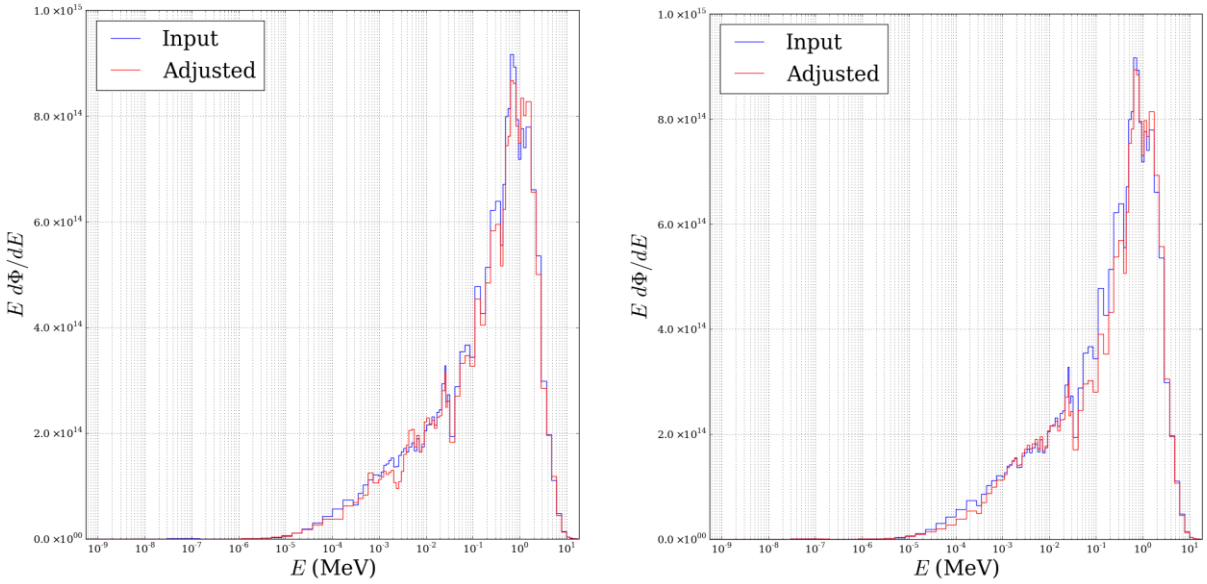

Fig. 5. Comparison of the adjustments performed using the 89 energy group structure for LSL-M2 (left) and GenSpec (right) for the LB44 environment in the central cavity of the ACRR.

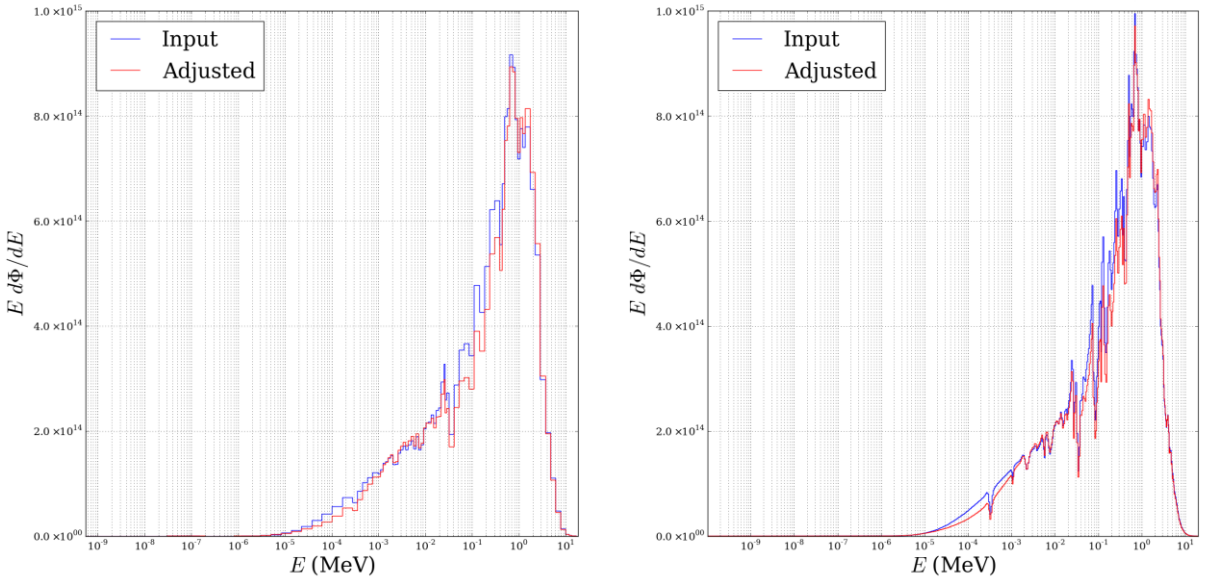

Fig. 6. Comparison of the adjustments performed using GenSpec for the 89 group (left) and 640 group (right) structures for the LB44 environment in the central cavity of the ACRR.

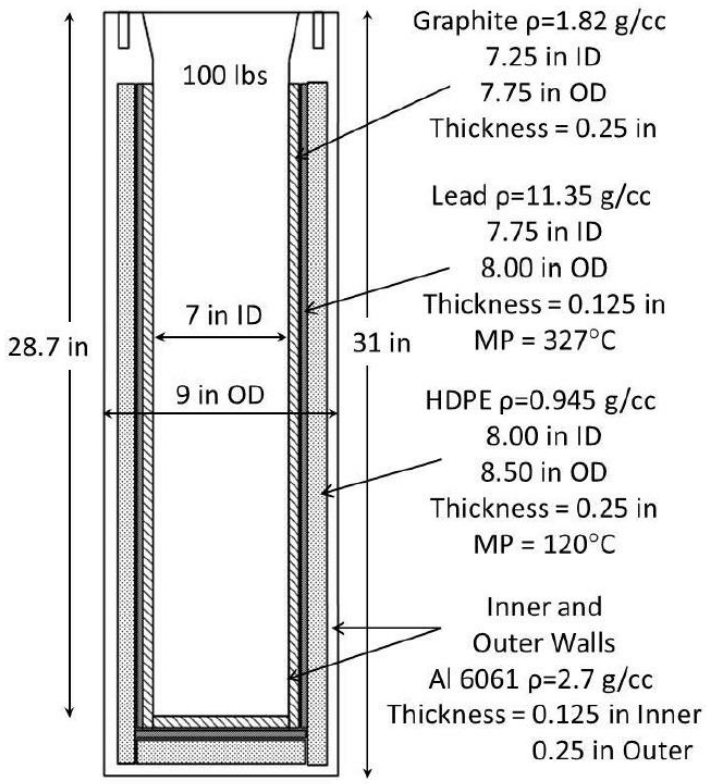

Fig. 7. Details of the PLG bucket.

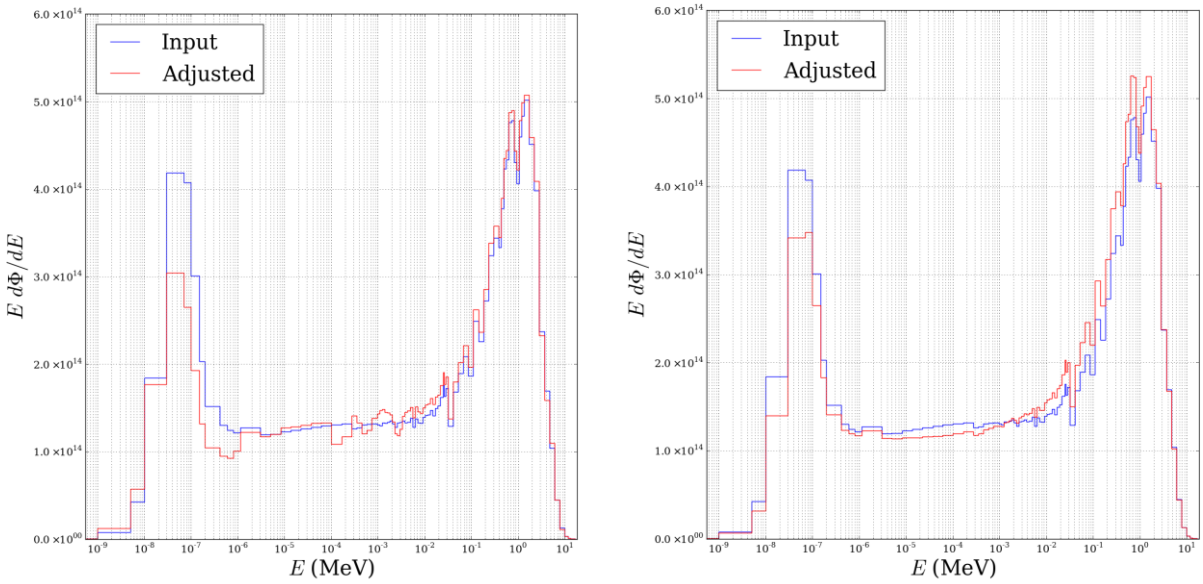

Fig. 8. Comparison of the adjustments performed using the 89 energy group structure for LSL-M2 (left) and GenSpec (right) for the PLG environment in the central cavity of the ACRR.

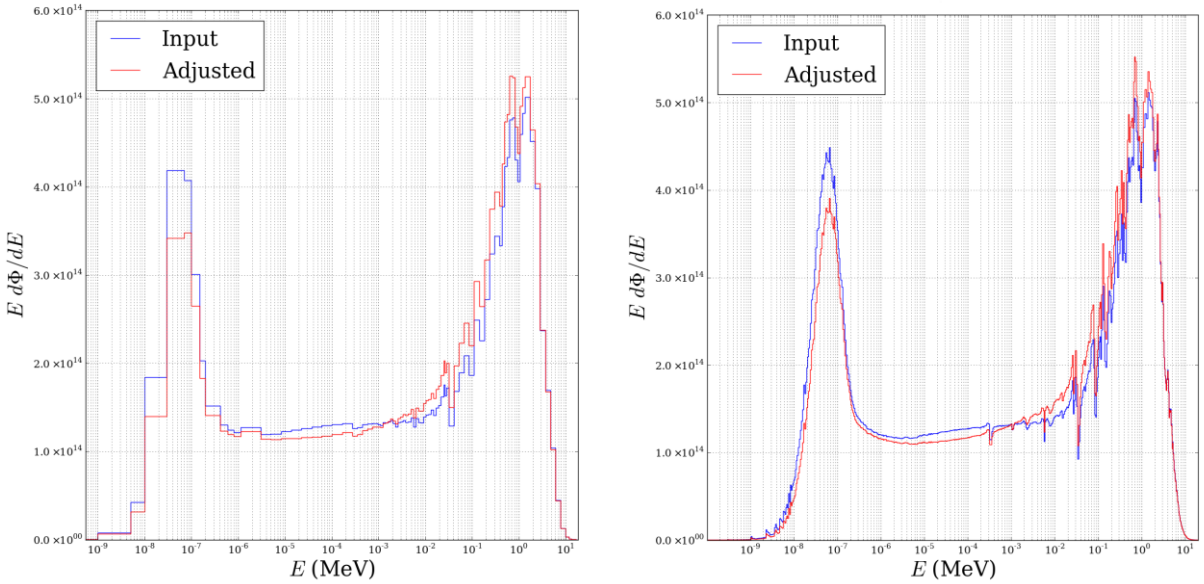

Fig. 9. Comparison of the adjustments performed using GenSpec for the 89 group (left) and 640 group (right) structures for the PLG environment in the central cavity of the ACRR.

Table 1. Comparison of the reaction probabilities predicted by LSL-M2 and GenSpec for the free field ACRR environment.

Reaction-Cover	LSL	GenSpec	Measured	LSL % diff	GenSpec % diff
na23g#-pelt-bahl	1.53E-10	1.54E-10	1.45E-10	6.157	6.818
na23g#-pelt-cdhl	3.33E-11	3.31E-11	3.34E-11	0.338	0.93
mg24p#-mil5-bahl	9.99E-13	1.02E-12	1.00E-12	0.27	1.949
al27a#-ml3x-bahl	4.70E-13	4.78E-13	4.79E-13	1.853	0.205
sc45g#-mil5-bahl	7.95E-09	7.97E-09	7.64E-09	4.039	4.25
sc45g#-mil5-cdhl	1.19E-09	1.23E-09	1.20E-09	0.568	2.569
ti46p#-milx-bahl	8.14E-12	8.20E-12	8.20E-12	0.689	0.026
ti47p#-milx-bahl	1.55E-11	1.55E-11	1.59E-11	2.48	2.204
ti48p#-milx-bahl	2.03E-13	2.06E-13	2.01E-13	1.253	2.891
mn55g#-mil2-bahl	4.59E-09	4.56E-09	4.65E-09	1.303	1.895
mn55g#-mil2-cdhl	1.24E-09	1.23E-09	1.23E-09	1.121	0.132
fe54p#-mil5-bahl	6.33E-11	6.32E-11	6.60E-11	4.071	4.242
fe56p#-mil5-bahl	7.43E-13	7.57E-13	7.80E-13	4.76	3.041
fe58g#-mil5-bahl	4.68E-10	4.58E-10	4.62E-10	1.434	0.737
fe58g#-mil5-cdhl	1.38E-10	1.29E-10	1.40E-10	1.599	7.511
co59p#-mil2-cdhl	1.01E-12	1.01E-12	9.96E-13	0.862	1.277
ni58p#-milx-bahl	8.63E-11	8.63E-11	8.63E-11	0	0
ni60p#-milx-bahl	1.50E-12	1.52E-12	1.52E-12	0.856	0.287
zn64p#-milx-bahl	3.04E-11	3.03E-11	3.17E-11	3.918	4.161
zr902#-milx-bahl	6.96E-14	6.97E-14	6.96E-14	0.04	0.056
nb932#-mil5-bahl	3.15E-13	3.05E-13	3.23E-13	2.431	5.567
w186g#-mil6-bahl	2.73E-08	2.72E-08	2.72E-08	0.276	0.026
au197g#-dil3-bahl	1.85E-07	1.88E-07	1.90E-07	2.548	1.281
au197g#-dil3-cdhl	1.59E-07	1.61E-07	1.59E-07	0.11	1.421
np237f#-void-fisa	1.57E-09	1.60E-09	1.58E-09	0.463	1.089
mo98g#-mil5-bahl	8.42E-10	8.53E-10	8.51E-10	1.127	0.16
mo98g#-mil5-cdhl	8.11E-10	8.22E-10	8.05E-10	0.702	2.095
s32cf#-void-bare	7.43E-02	7.41E-02	7.04E-02	5.54	5.259
rmleu#-rmle-fiss	2.90E-09	2.68E-09	3.14E-09	7.66	14.692
rmldu#-rmld-fiss	2.79E-10	2.82E-10	2.85E-10	2.202	1.278
rmlpu#-rmlp-fiss	3.33E-09	3.17E-09	3.16E-09	5.602	0.341

Table 2. Comparison of the reaction probabilities predicted by LSL-M2 and GenSpec for the LB44 environment in the ACRR central cavity.

Reaction-Cover	LSL	GenSpec	Measured	LSL % diff	GenSpec % diff
na23g#-pelt-bare	1.08E-11	1.28E-11	9.97E-12	8.293	28.757
al27p#-void-bare	2.61E-12	2.49E-12	2.82E-12	7.406	11.651
al27a#-void-bare	4.13E-13	4.05E-13	4.10E-13	0.762	1.075
sc45g#-mil5-bare	1.78E-10	1.73E-10	1.75E-10	2.029	1.109
ti46p#-void-bare	7.52E-12	7.17E-12	7.02E-12	7.102	2.1
ti47p#-void-bare	1.57E-11	1.59E-11	1.51E-11	4.004	5.189
ti48p#-void-bare	1.79E-13	1.75E-13	1.76E-13	1.604	0.617
mn55g#-wcu2-bare	5.62E-10	4.87E-10	5.44E-10	3.28	10.54
mn552#-void-bare	1.20E-13	1.22E-13	1.36E-13	11.624	10.373
fe54p#-void-bare	6.10E-11	6.08E-11	5.82E-11	4.702	4.397
fe56p#-void-bare	6.64E-13	6.43E-13	6.43E-13	3.175	0.007
fe58g#-mil5-bare	6.58E-11	5.61E-11	6.90E-11	4.589	18.648
fe58g#-void-fiss	1.70E-11	1.58E-11	1.55E-11	10.213	2.031
co592#-void-bare	1.18E-13	1.20E-13	1.11E-13	6.567	8.098
co59g#-mil2-bare	1.54E-09	1.52E-09	1.50E-09	2.882	1.045
co59g#-void-fiss	5.14E-11	4.91E-11	5.04E-11	2.073	2.575
co59p#-void-bare	9.40E-13	8.99E-13	9.14E-13	2.828	1.687
ni58p#-void-bare	8.47E-11	8.47E-11	8.47E-11	0	0
ni60p#-void-bare	1.37E-12	1.31E-12	1.30E-12	5.568	0.904
cu63g#-void-bare	4.30E-10	3.98E-10	4.39E-10	1.996	9.448
nb932#-void-bare	2.61E-13	2.56E-13	2.56E-13	1.941	0.006
in115n#-void-bare	2.19E-10	2.22E-10	2.29E-10	4.542	3.322
in115g#-mil5-bare	2.43E-09	2.31E-09	2.10E-09	15.907	10.414
au197g#-dil5-bare	8.55E-09	6.85E-09	8.16E-09	4.797	16.076
au197g#-void-fiss	8.61E-10	8.33E-10	9.12E-10	5.577	8.729
u235f#-void-fisa	3.96E-09	3.81E-09	3.80E-09	4.003	0.124
np237f#-void-fisa	1.98E-09	1.98E-09	1.98E-09	0.454	0.026
pu239f#-void-fisa	4.59E-09	4.44E-09	4.55E-09	0.912	2.426
mo98g#-mil5-bare	5.97E-10	5.75E-10	5.64E-10	5.772	1.882
mo98g#-void-fiss	1.63E-10	1.57E-10	1.36E-10	19.484	15.5
u238f#-void-fisa	2.96E-10	3.01E-10	2.89E-10	2.411	4.425

Table 3. Comparison of the reaction probabilities predicted by LSL-M2 and GenSpec for the PLG environment in the ACRR central cavity.

Reaction-Cover	LSL	GenSpec	Measured	LSL % diff	GenSpec % diff
na23g#-pelt-bahl	3.24E-10	3.17E-10	3.06E-10	6.096	3.8
na23g#-pelt-cdhl	3.36E-11	3.50E-11	3.25E-11	3.509	7.855
mg24p#-mil5-bahl	8.02E-13	8.37E-13	7.66E-13	4.64	9.292
al27a#-ml3x-bahl	3.74E-13	3.91E-13	3.77E-13	1.003	3.612
sc45g#-mil5-bahl	1.80E-08	1.73E-08	1.73E-08	4.02	0.099
sc45g#-mil5-cdhl	1.30E-09	1.35E-09	1.35E-09	4.104	0.049
ti46p#-milx-bahl	6.69E-12	6.64E-12	6.40E-12	4.575	3.773
ti47p#-milx-bahl	1.24E-11	1.24E-11	1.27E-11	2.17	1.963
ti48p#-milx-bahl	1.64E-13	1.69E-13	1.63E-13	0.791	3.724
mn55g#-mil2-cdhl	1.49E-09	1.42E-09	1.49E-09	0.132	4.839
mn552#-mil2-bahl	1.17E-13	1.11E-13	1.38E-13	15.21	19.572
fe54p#-mil5-bahl	5.03E-11	5.03E-11	4.97E-11	1.235	1.137
fe56p#-mil5-bahl	6.12E-13	6.18E-13	6.20E-13	1.359	0.288
fe58g#-mil5-bahl	9.77E-10	9.33E-10	9.34E-10	4.686	0.05
fe58g#-mil5-cdhl	1.55E-10	1.50E-10	1.49E-10	3.495	0.728
co592#-mil2-cdhl	1.13E-13	1.07E-13	1.12E-13	0.776	4.378
co59g#-mil2-bahl	2.80E-08	2.73E-08	2.72E-08	2.636	0.264
co59g#-mil2-cdhl	5.39E-09	5.73E-09	5.33E-09	1.069	7.473
co59p#-mil2-cdhl	8.21E-13	8.16E-13	8.16E-13	0.62	0.014
ni582#-milx-cdhl	2.32E-15	2.16E-15	2.15E-15	7.732	0.215
ni58p#-milx-bahl	6.88E-11	6.88E-11	6.88E-11	0	0
ni60p#-milx-cdhl	1.23E-12	1.23E-12	1.25E-12	2.066	2.283
cu63g#-mil5-bahl	3.31E-09	3.19E-09	3.31E-09	0.012	3.587
cu63g#-mil5-cdhl	5.11E-10	5.27E-10	4.98E-10	2.738	5.928
cu63a#-mil5-cdhl	2.97E-13	2.98E-13	3.60E-13	17.351	17.034
zn64p#-milx-bahl	2.40E-11	2.41E-11	2.45E-11	1.942	1.756
zr902#-milx-bahl	5.66E-14	5.27E-14	5.75E-14	1.622	8.338
nb932#-mil5-bahl	2.44E-13	2.44E-13	2.41E-13	1.089	1.117
in115n#-mil5-bahl	1.55E-10	1.56E-10	1.65E-10	6.386	5.446
au197g#-dil3-bahl	2.44E-07	2.34E-07	2.40E-07	1.416	2.601
au197g#-dil3-cdhl	1.80E-07	1.73E-07	1.79E-07	0.76	3.088
mo98g#-mil5-bahl	8.84E-10	8.46E-10	8.67E-10	1.95	2.404
mo98g#-mil5-cdhl	8.04E-10	7.70E-10	7.98E-10	0.692	3.544
s32cf#-void-bare	5.85E-02	5.88E-02	5.44E-02	7.537	8.052
rmleu#-rmle-fiss	2.46E-09	2.57E-09	2.57E-09	4.362	0.053
rmldu#-rmld-fiss	2.25E-10	2.27E-10	2.19E-10	2.631	3.473
rmlpu#-rmlp-fiss	2.79E-09	2.92E-09	2.57E-09	8.627	13.482